LAWRENCE
LIVERMORE
NATIONAL
LABORATORY

LLNL-JRNL-839225

Estimation of CFETR performance and burning fraction in different pellet fueling scenarios by a multi-species radial transport model

W. S. Lin, X. G. Wang, X. Q. Xu

August 25, 2022

Plasma Sci. Technol.

Estimation of CFETR performance and burning fraction in different pellet fueling scenarios by a multi-species radial transport model

W S Lin[1]‡, X G Wang[2], X Q Xu[3],D F Kong[4], Y M Wang[4],J L Chen[4],Z H Wang[5], C J Xiao[1]

[1] State Key Lab of Nuclear Physics & Technology and School of Physics, Peking University, Beijing 100871,People's Republic of China

[2] Department of Physics, Institute of Space Environment and Matter Science, Harbin Institute of Technology, Harbin 150001, People's Republic of China

[3] Lawrence Livermore National Laboratory, Livermore, California 94551, USA

[4] Institute of Plasma Physics, Chinese Academy of Sciences, Hefei 230031, People's Republic of China

[5] Southwestern Institute of Physics, Chengdu 610041, People's Republic of China

E-mail: `xgwang@hit.edu.cn, 2018lws@pku.edu.cn`

Abstract. As an engineering test reactor, CFETR operation scenarios take the tritium recycling into account. A key factor to make tritium fuel self-sustainable is the burning fraction. In comparison to the Lawson ignition criterion, zero-dimensional (0-D) burning fraction analysis under low fueling efficiency and particle confinement time have the higher requirement on future ignited plasmas. To self-consistently simulate burning plasmas with profile changes in pellet injection scenarios and to estimate the corresponding burning fraction, a one-dimensional (1-D) multi-species radial transport model is developed in BOUT++ frame. Several pellet-fueling scenarios are then tested in the model. Results show that the increased fueling depth improving the burning fraction by particle confinement improvement and fusion power increase. Nevertheless, as increasing the depth, the pellet cooling-down may significantly lower the temperature in the core region. Taking the density perturbation into consideration, the reasonable parameters of the fueling scenario in this simulation are estimated as the pellet radius r_p=3mm, the injection rate = 4Hz, the pellet injection velocity = 1000m/s-2000m/s without drift or 450m/s with HFS drift.

Keywords: CFETR, scenario, Tritium burning fraction

1. Introduction

Tritium self-sustention in future DT fusion reactor is a crucial challenge. The daily tritium consumption for a fully operated Gaga-Watt (GW) fusion power station is on the order of kg. Thus, current annual tritium production in the world can only support

‡ Present address: Department of Physics, Peking University, No.5 Yiheyuan Road Haidian District , China.

the operation of such a power station for a couple of weeks or so. According to a recent tritium recycling model[1, 2],the burning fraction, which measures the percentage of tritium particles burned in one tritium cycle period, is a key factor for tritium self-sustention due to the low tritium breeding rate (TBR) predicted. Furthermore, the startup of tritium should be more than 10kg if the burning fraction is only 1

Thus, besides sustaining a steady-state density profile in ITER scenarios, achieving a high burning fraction should also be a target for China Fusion Engineering Test Reactor (CFETR) [3] fueling scenarios.

Different from existing experiment facilities and International Thermonuclear Experiment Reactor (ITER), CFETR requires a burning fraction of 3% for the goal to test the accessibility to the future fusion plant. The definition of the burning fraction is $f_b = \eta_f S_{fu}/S_{Tf}$, where S_{fu} is the fusion rate of tritium ions, S_{Tf} is the rate of tritium particles, and η_f is the efficiency making the fueling rate of tritium ions S_{Tf}/η_f. Therefore, the way to improve the burning fraction can be proposed as follows.

(1) Improving the fuel efficiency. The fueling efficiency η_f of gas puffing(GP)[4], supersonic molecular(SMBI)[5], pellet injection(PI)[6], CT[7] is about 1-10%,10-30%,>50%,>50%, respectively. The difference between these fueling methods comes from the process that they experience. GP and SMBI fuelings are mainly by diffusion, while for PI, the main processes are ablation and drift, and for CT the main process is magnetic reconnection. Due to high fueling efficiency, PI and CT have became the most possible options for CFETR. In this paper, we focus on pellet scenarios.

(2) Increasing the particle confinement time. The enhanced particle confinement was observed both in experiments and simulations by fueling at core region by neutral beam injection(NBI) or high speed PI[8, 9]. Typically, it was thought that the diffusion coefficient in the central core region is small, and thus center can help increase the particle confinement. This makes the fueling depth a key factor for CFETR fuel system design.

(3) Raising the energy confinement level. Besides sustaining the density, fueling is also a method to control burning plasma[10]. For a GW fusion reactor, the schematic flowchart of particle and power flows of burning plasmas in tritium recycling is illustrated in Fig. 1. As PI or CT injected into plasma, the plasma density increases and temperature cools down, which directly affects the alpha heating and plasma confinement, with $\tau_{E98} \propto n^{0.41} P^{-0.69}$, where n is the average density and P is effective heating power. In fact, the interaction between alpha and background particles causes multi-scale spatial-temporal fluctuations[11]. For simplicity, in this paper, the interaction between them is represented by τ_{E98} as illustrated in Section 3.

Considering these factors to achieve the high tritium burning fraction thus becomes a central for studies of CFETR and other future DEMO operations. We then in this paper self-consistently simulate burning plasmas with profile changes in pellet injection scenarios and estimate their burning fraction in a one-dimensional (1-D) multi-species radial transport model developed in BOUT++ framework. Various pellet-scenarios are tested in the model. Results show that the increased depth improving the burning fraction by particle confinement improvement and fusion power increase. Also, operation parameters for reasonable scenarios are estimated.

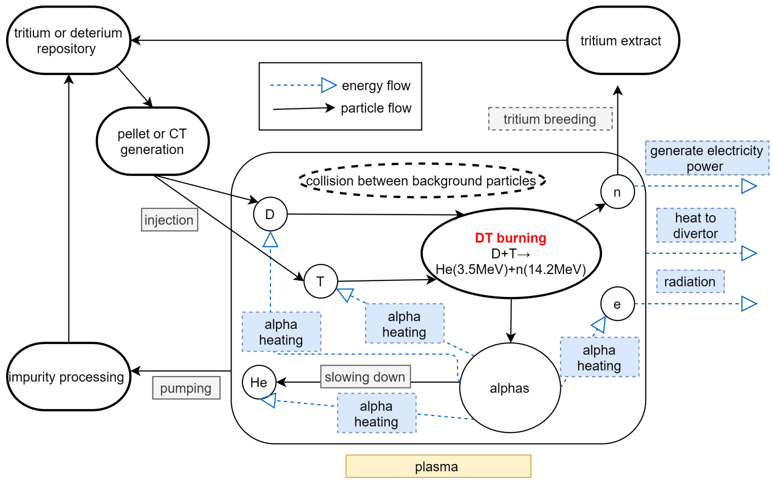

Figure 1: Illustration of the particle flow and energy flow at burning plasma tritium recycling

The layout of the paper is as follows. In Section 2, we first start from 0D burn fraction model to make a magnitude estimation of requirement for future reactor design. Then, a 1D radial transport model introduced in our previous work[12] is modified to take the temperature profile evolution into account and with the pellet deposition described by the neutral gas (NGS) and magnetohydrodynamic (MHD) drift model. This extended transport model with boundary conditions and CFETR parameters applied are described in Section 3. The fueling scenario design, a short review of the pellet NGS-MHD model, and numerical results of different PI fueling scenarios are shown in Section 4. Finally, summary and discussion are presented in Section 5.

2. 0D burn fraction criterion

Before considering the complicated processes in burning plasma in the 1-D simulation as shown inFig. 1, a simple 0-D analysis is used for magnitude analysis of the burning fraction in future reactor design.

Let us rewriting the definition of the ideal burning fraction as

$$f_b = \frac{S_{fu}}{S_T} \approx \frac{\frac{1}{4}n^2 < \sigma v > V}{S_T} = \frac{n\tau_E < \sigma v > \eta_f}{2\gamma} \geq f_c \tag{1}$$

where $S_T = S + S_{fu}$ with tritium ion loss rate $S = N/2\eta_f\tau_p \gg S_{fu}$ in magnetic fusion reactors, N is the total ion number(D + T with 1/2 ratio) and V is the volume of the plasma with the plasma density $n = N/V$, while τ_E is the energy confinement time and τ_p is the particle confinement time with their ratio $\gamma \equiv \tau_E/\tau_p$; as well as $< \sigma v >$

is the average fusion reaction cross-section and f_c is the critical burning fraction. This gives the constraint for future reactor

$$n\tau_E \geq \frac{2f_c\gamma}{<\sigma v>\eta_f} \tag{2}$$

We then call it "the burning fraction criterion" to compare with the well-known "Lawson ignition criterion" which has a similar form of

$$n\tau_E \geq \frac{3T}{<\sigma v>E/20-\lambda T^{0.5}} \tag{3}$$

derived from

$$P_\alpha = \frac{P_r}{5} = \frac{n^2<\sigma v>E_\alpha}{20} \geq P_L = P_b + \frac{3nT}{\tau_E} \tag{4}$$

where λ is the radiation coefficient,$P_\alpha, P_r, P_L, P_b = n^2\lambda T^{0.5}$ are alphas, fusion reaction, loss, bremsstrahlung radiation powers per unit volume,respectively. It should be noted that in long duration steady-state operations, the fueling particles need to be heated to background plasma temperature, which contributes additional loss of energy. Thus the modification to ignition condition will be:

$$P_L = P_b + \frac{3nT}{\tau_E} + 2ST/V \tag{5}$$

leading to a "modified ignition criterion"

$$n\tau_E \geq \frac{(3+\gamma/\eta_f)T}{<\sigma v>E/20-\alpha T^{0.5}} \tag{6}$$

The real situation falls between the Eq. (3) and Eq. (6), due to some particles being already lost before totally heated. The typical value of γ in tokamaks is 0.25-0.6,radiation coefficient is 4.9×10^{-37} and f_c is chosen equal to 3%.

We then investigate certain cases with typical confinement and fueling efficiency parameters to analyse their effects on the criterions. It is found that, for the high particle confinement($\gamma = 0.25$) and high efficiency($\eta_f = 0.8$), the burning fraction criterion is far below the ignition criterion when temperature is 10-20keV as shown in Fig. 2(a). And the modified criterion is almost the same as the Lawson ignition criterion. In this case, the way to fusion energy comes back to improving the energy confinement, studied for decades. However, when the particle confinement($\gamma = 0.6$) is low but with high efficiency($\eta_f = 0.8$) or the particle confinement ($\gamma = 0.25$) is high but with low efficiency($\eta_f = 0.1$), the criterion curves of burning fraction and ignition cross at $T \sim 10-20keV$, which can be seem in Fig. 2(b) and (c). And the cooling down effect due to fueling particles heating can be visible from difference between Lawson ignition criterion and the modified ignition criterion. In Fig. 2(d),the low particle confinement ($\gamma = 0.6$) and low efficiency($\eta = 0.1$) work together to worsen the situation. The lowest of burning fraction criterion is shown at the $\sim 30keV$, beyond the requirement of ignition condition as usually expected. And the cooling down of fueling particles cannot not be ignorable.

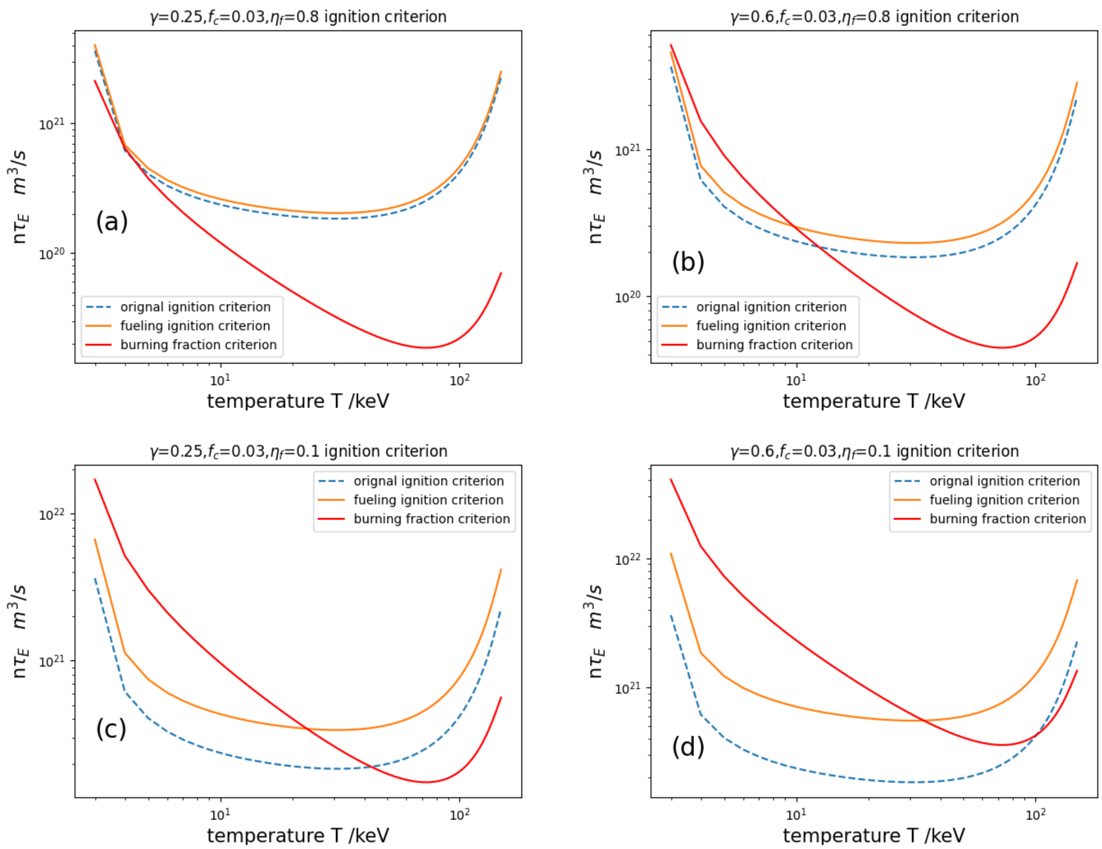

Figure 2: 0D ignition conditions with certain typical particle confinement and fueling efficiency parameters:(a)$\eta_f = 0.8, \gamma = 0.25$.(b)$\eta_f = 0.8, \gamma = 0.6$.(c)$\gamma = 0.25, \eta = 0.1$.(d)$\gamma = 0.6, \eta = 0.1$.

It is more convenient to analyse pre-ignition plasma by introducing the energy gain factor

$$Q = \frac{P_r}{P_{heat}} = \frac{<\sigma v> n^2 V E_\alpha}{P_{heat}} = \frac{<\sigma v> n P E_\alpha}{4 T_i P_{heat}} \tag{7}$$

$$\tau_E = \frac{P}{P_{heat}(1 + Q/5)} \tag{8}$$

$$f_b = \eta_f \frac{T_i}{\gamma E_\alpha} \frac{10Q}{5 + Q} \tag{9}$$

where P_{heat} is auxiliary heating power. It can be clearly seen from Eq. (9) that the factors affecting burn fraction are the ion temperature T_i, the energy gain Q and the confinement ratio of energy to particle $\gamma = \tau_E/\tau_p$. Although the 0-D model casts light on the way to raise the burning fraction, the profile effect and the correlations among Q,T_i and γ can't be described without the transport analysis. Therefore, 1-D radial transport model need to be simulated to find the reasonable fueling scenarios for CFETR.

3. The 1D Transport Model And Numerical Setups

3.1. Basic Equations

As mentioned above, the burning plasma transport problem is a complicated problem due to taking fusion reaction and fuel source terms into account at the same time. Let's start from collisional kinetic equation for the distribution function f_s with s stands for the different species,

$$\frac{\partial f_s}{\partial t} + v \cdot \nabla f_s + \frac{q}{m}(E + \frac{v \times B}{c}) \cdot \frac{\partial f_s}{\partial v} = C + A + P \tag{10}$$

where C,A,F are collision, fusion reaction and fueling source terms, respectively.

While the kinetic simulation is time-consuming[13] in computation and the momentum of fueling source term is hardly estimated both in theory and experiment, the reduced Braginskii[14] equations are then used in our model with source and sink terms due to fueling and fusion reaction. As be introduced previously[12] and take the thermal transport into account, the set of model equations are thus written

$$\frac{\partial n_{D,T}}{\partial t} + \nabla \cdot \Gamma_{D,T} = S_{D,T} - S_{fu} \tag{11}$$

$$\frac{\partial n_{\alpha}}{\partial t} + \nabla \cdot \Gamma_{\alpha} = S_{fu} - \frac{n_{\alpha}}{\tau_s} \tag{12}$$

$$\frac{\partial n_{He}}{\partial t} + \nabla \cdot \Gamma_{He} = \frac{n_{\alpha}}{\tau_s} \tag{13}$$

$$n_e = n_D + n_T + 2n_{He} + 2n_{\alpha} \tag{14}$$

$$\frac{3}{2}\frac{\partial T_{D,T}}{\partial t} = -\frac{3}{2}u_{D,T}\nabla T_{D,T} - \nabla q_{D,T} - T_{D,T}\nabla u_{D,T} + P_{\alpha D,\alpha T} + P_{aux} + Q_{D,T} - \frac{3}{2}S_{D,T}T_{D,T} \tag{15}$$

$$\frac{3}{2}\frac{\partial T_{He}}{\partial t} = -\frac{3}{2}u_{He}\nabla T_{He} - \nabla q_{He} - T_{He}\nabla u_{He} + P_{\alpha He} + P_{auxHe} + Q_{He} \tag{16}$$

$$\frac{3}{2}\frac{\partial T_e}{\partial t} = -\frac{3}{2}u_e\nabla T_e - \nabla q_e - T_e\nabla u_e + P_{\alpha e} + P_{auxe} - P_{rad} + Q_e - \frac{3}{2}S_eT_e \tag{17}$$

where the term $S_{D,T}$ is the PI source term, as described in Sub-Section 4.2. The fueling efficiency of PI is assumed 100% and the D:T ratio is 50%:50% for simplicity. The reasoning of this assumption is based on the high density and the temperature pedestal of CFETR. Also, P_{aux} is the auxiliary heating power and $S_{fu} = n_D n_T \langle \sigma_{DT} v \rangle$ is the loss term for D,T ions due to fusion reaction. The classical slowing down theory[15] for alphas is consistent with DT experiments in TFTR and JET without obvious alphas driven Alfven eigenmode(AE) activities observed[16]. It may not be the case for CFETR due to the large population of alphas and AE induced transport. Thus, in this paper classical slowing down is only an approximation for alphas confinement. The detailed formula for the slowing down time τ_{slow}, alpha heatingP_{α}, and heat transfer due to collision Q_s are discussed in Appendix Appendix A. The particle flux Γ, effective velocity u, and thermal flux q are illustrated as below.

3.2. Setting for fluxes

To simplify the model, the form of species thermal flux is set as in the COREDIV CFETR simulation[17], for CFETR 1GW scenario profile that calculated by OMFIT[18] with TGYRO[19] and TGLF[20]. For the thermal species ($s = D, T, He, e$) in the background plasma, fluxes are set as follows,

$$\Gamma_s = -D_s \nabla n_s + n_s V_s \tag{18}$$

$$q_s = -n_s \chi_s \nabla T_s \tag{19}$$

And the corresponding particle transport coefficient D_s, the heat conductivity χ_s and the inward pinch velocity V_s are then writtern

$$D_s(D_\parallel \gg D_\perp) = D_{s\perp} = 0.35\chi_s \tag{20}$$

$$\chi_s = \frac{2C_{ei}a^2}{\tau_{E\_\_98}}[0.1 + 0.9\left(\frac{r}{a}\right)^4]F(r) \tag{21}$$

$$F(r) = (1-A)e^{-\left(\frac{r}{a\rho_0}\right)^{2p}} + A \tag{22}$$

$$V_s = 2C_v \frac{r}{a^2} D_s \tag{23}$$

where the parameter $A = 0.1$, $\rho_0 = 0.92$, $p = 100$, $C_ei = 1$, $C_v = 0.65$, and a is the minor radius. The combination of alphas and thermal species in global transport is based on τ_{E_98}, where the fusion power and the effective mass enter the formula as

$$\tau_{E\_\_98} = 0.0562 I^{0.93} B^{0.15} P^{-0.69} \overline{n}^{0.41} \overline{M}^{0.19} R^{1.97} \varepsilon^{0.58} \kappa^{0.78} \tag{24}$$

$$\overline{n} = \frac{\int_V n_e J d\psi d\theta d\xi}{\int_V J d\psi d\theta d\xi} \tag{25}$$

$$\overline{M} = \frac{\int_V \frac{4n_\alpha + 4n_{He} + 2n_D + 3n_T}{n_\alpha + n_{He} + n_D + n_T} J d\psi d\theta d\xi}{\int_V J d\psi d\theta d\xi} \tag{26}$$

$$P = P_{cd} + P_\alpha = P_{aux} + S_{fu} W_{\alpha 0} - P_{rad} \tag{27}$$

where P_α is the fusion power. The diffusion and pinch of alphas differ from the other species due to the its isotropic velocity at $W_{\alpha 0} = 3.5MeV$. The method dealing with the alphas is based on the quasilinear model by Angioni et al. for study of turbulent transport of alphas and helium ash [21]. The alpha particle diffusion and pinch can be expressed as

$$\Gamma^\alpha_{ITG/TEM} = -D^\alpha_{ITG/TEM} \frac{dn_\alpha}{dr} = n_\alpha D_\alpha [\frac{1}{L^\alpha_n} + \frac{C_p}{R}] \tag{28}$$

$$D_\alpha = D_{He}[0.02 + 4.5\frac{T_e}{E_\alpha} + 8\left(\frac{T_e}{E_\alpha}\right)^2 + 350\left(\frac{T_e}{E_\alpha}\right)^3] \tag{29}$$

$$C_p = \frac{3}{2}\left(\frac{R}{L_{Te}}\right)\{1/[(1 + 1/W_c^{1.5})\log(1 + 1/W_c^{1.5})] - 1\} \tag{30}$$

where L^α_n and L_{Te} are the characteristic lengths of alpha particle density and electron temperature profiles, respectively.

Table 1: CFETR design parameters

Major radius $R(m)$	Minor radius $a(m)$	Toroidal field $B(T)$	Plasma current $I_p(MA)$	Current drive power $P_{cd}(MW)$	Vertical elongation κ	RF heating $P_{RF}(MW)$	NBI heating $P_{NBI}(MW)$	Radiation power $P_{rad}(MW)$
7.2	2.2	6.5	13.0	74	2.03	60	20	115.6

3.3. CFETR parameters and boundary condition

Several CFETR GW operation scenarios have been designed in integrated modeling by CFETR Physics Team[22]. We then in this paper apply a GW hybrid scenario with corresponding CFETR parameters are shown at Table 1. While the heavy impurity transport effect is not considered in this paper, the impurity radiation power is however taken into account and fixed in the simulation. The radiation, and NBI heating power profiles are shown in Fig. 3.

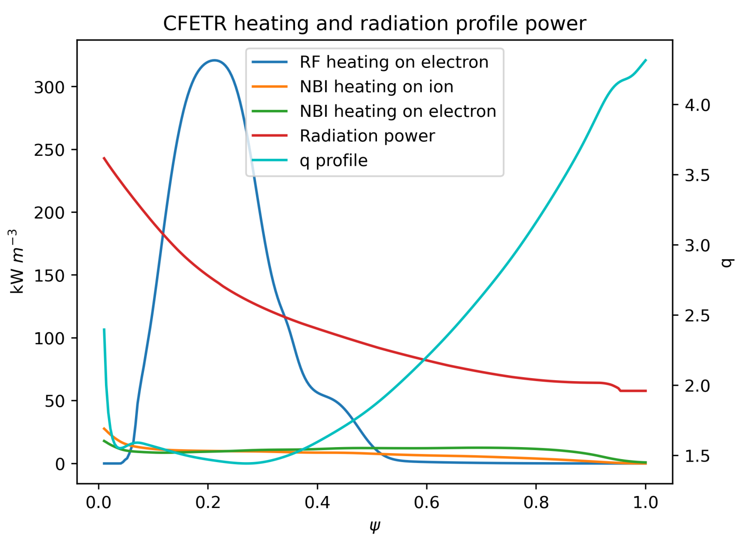

Figure 3: CFETR 1GW hybrid scenario RF ,NBI heating and radiation profile

The simulation is conducted under the framework of BOUT++[23] in the region of $\psi = (0.01, 1.0)$. The inner boundary condition is set as Neumann condition for both plasma density and temperature. For the outer boundary condition, the strong pumping and low particle recycling conditions are assumed to avoid the increase of the boundary neutral gas pressure and to reduce the plasma-wall interaction(PWI). The high recycling wall and weak pumping condition are believed to have deleterious effect on confinement as external gas puffing, which is verified in ASDEX experiment[24]. Therefore, the density and temperature are keep fixed value at edge and the pinch velocity is set zero for no edge particle inflow. Thus, on the outer boundary we have

$$n_D|_{edge} = n_T|_{edge} = 1.4{\times}10^{19}m^{-3}, n_{He}|_{edge} = n_\alpha|_{edge} \approx 0, and V_{pinch}|_{edge} \approx 0 \quad (31)$$

4. Simulation results for different fueling scenario

4.1. Fueling scenario design

For the priority of a >3% burning fraction at CFETR fueling system, pellet injection and compact torus are the most possible fueling method for the fueling efficiency as stated in Section 1. And the tritium fueling rate required by 1GW fusion power with a burning fraction of 3%, can be estimated by $P_{fusion}/E_{fusion}/f_b = 1GW/17.6MeV/3\% \approx 1.18 \times 10^{22}$. However, considering the tritium fueling rate of CT of one shot is about 1mg, i.e., 2.4×10^{20} particles, hard to balance the particle loss(burning + diffusion) throughout in CFETR, the PI fueling is considered at first.

4.2. Pellet fueling scenario

In this subsection, we focus on the different PI effects on CFETR density and temperature profiles, as well as corresponding burning fractions and fusion powers. Assuming the pellet density $n_p = 5.96 \times 10^{22} cm^{-3}$, the tritium fueling rates for different pellet sizes and PI frequencies are shown in Table 2. The tritium fueling rate about 1.18×10^{22} per second(the bold text in Table 2) is selected in our simulation. The PI velocity are $v_p = 500m/s$, $1000m/s$, $1500m/s$, and $2000m/s$ without pellet drift. And for high-field-side(HFS) cases, the tube curvature of PI limits the injection velocity. Thus, the HFS pellet velocity are chosen $v_p = 150m/s$,$300m/s$,$450m/s$.

Main PI processes are pellet ablation and deposition, as well as ablated materials drift and parallel expansion[6]. For the pellet deposition, the NGS model is used, which is widely verified at international pellet ablation database(IPADBASE)[25].The pellet deposition profile is then calculated by the NGS model as follows[26],

$$\frac{dr_p}{dt} = 1.72 \times 10^{-8} r_p^{-2/3} n_{e0}^{1/3} T_{e0}^{1.64} cm/sec \quad (32)$$

$$T_* = 1.12 \times 10^{-8} r_p^{2/3} n_{e0}^{2/3} T_{e0}^{-0.14} eV \quad (33)$$

$$r_{cloud} = 1.54 \times 10^4 (T_e/M_i)^{1/6} (4\epsilon T_* + E_{ion} + E_{diss}) r_p^{2/3} (n_e \ln \Lambda_{en})^{-1/3} \quad (34)$$

$$S_{D,T} = \frac{dN_p}{dx} = \frac{4\pi r^2 n_p dr}{v_p dt} \quad (35)$$

where T_* stands for the temperature at the sonic radius and r_{cloud} is characteristic length of the cloud. Also, ϵ, E_{ion}, E_{diss}, $\ln \Lambda_{en}$ are constants in our simulation.

The drift phenomenon of ablated material is widely observed at ASDEX, JET, DIII-D and other tokamaks[6, 27]. The drift of ablated cloud toward major radius

Table 2: Tritium fueling rate under different scenarios

fueling rate(s^{-1}) f(Hz) / r_p(cm)	16	12	8	4	2	1
0.2	$\mathbf{1.6 \times 10^{22}}$	$\mathbf{1.2 \times 10^{22}}$	$\mathbf{7.98 \times 10^{21}}$	3.99×10^{21}	2×10^{21}	9.98×10^{20}
0.3	5.39×10^{22}	4.04×10^{22}	$\mathbf{2.69 \times 10^{21}}$	$\mathbf{1.35 \times 10^{22}}$	$\mathbf{6.74 \times 10^{21}}$	3.36×10^{21}
0.4	1.28×10^{23}	9.58×10^{22}	6.39×10^{22}	3.19×10^{22}	$\mathbf{1.6 \times 10^{22}}$	7.98×10^{21}
0.5	2.5×10^{23}	1.87×10^{23}	1.25×10^{23}	6.24×10^{22}	3.12×10^{22}	$\mathbf{1.56 \times 10^{22}}$

direction is related to the toroidal curvature. And the displacement due to the drift can be estimated by the MHD model[28] as:

$$\frac{\delta\psi_0}{\psi} = \frac{R\delta\phi}{\psi} = q\beta B\cos\theta(1+\frac{qL_c}{a})^{-1}\frac{R}{a}\frac{\delta n r_0^2}{(n+\langle\delta n\rangle)}\frac{1}{\phi_{bndry}-\phi_{axis}} \tag{36}$$

$$S_{D,T}(\psi) \rightarrow S_{D,T}(\psi+\delta\psi) \tag{37}$$

where $L_c = (r_p R)^{1/2}$ is the characteristic length in the toroidal direction, $\delta n = \frac{\delta N}{\pi r_{cloud}^2 L_c}$ is the deposited density in the ablated cloud region and $\langle\delta n\rangle = \frac{\delta N}{4\pi^2 \mathrm{aRr_{cloud}}}$ is the increased density after the local deposited materials fully is flatten in the toroidal and poloidal directions. Note that ψ is the poloidal flux in BOUT++, while $\phi = \psi/R$ is the poloidal flux in MHD model. This MHD model also assumes that all particles in the pellet take part in drift dynamic result, which overestimates the drift displacement. Actually, once the pellet cloud expand to half poloidal cycle, the poloidal current connection damps the drift[29]. Moreover, the resistance and the nonlinear interaction between the background plasma and the pellet cloud also reduce the drift displacement. A more complicated theoretical model for drift effect with detailed physics can be found in Park's work.[30] To aviod overestimate the drift effect, the damp factor $b = 2$ is introduced, leading to $\delta\psi = \delta\psi_0(1-e^{-b})$. The Eq. (37) maps the no drift profile Eq. (35) into the drifted profile.

The time-scale of parallel expansion is typically less than 1ms, shorter than the radial profile transport time-scale concerned. Thus the detailed parallel expansion process is not included in our simulation to reduce the problem into 1-D. Based on these assumptions the simulation is carried out and resluts are described as follows.

4.2.1. The size and drift effects of PI on profile evolution Two typical cases are compared in this subsection, one for $r_p = 2mm$, $f = 16Hz$, the other for $r_p = 5mm$, $f = 1Hz$, also with the $v_p = 150m/s$ in the HFS and $v_p = 500m/s$ in the no drift cases. Then, the total tritium fueling rate(the number of total particles injected per seconds) is almost the same in the two cases, as shown in Table 2. It is clearly seen in Fig. 4(a) that the steady state electron density of $r_p = 5mm$ scenarios is much higher than that of $r_p = 2mm$ scenarios. And in a pellet period, the fluctuation of the average density of $r_p = 5mm$ scenarios is about $2 \times 10^{19} m^3$. However, the fluctuation

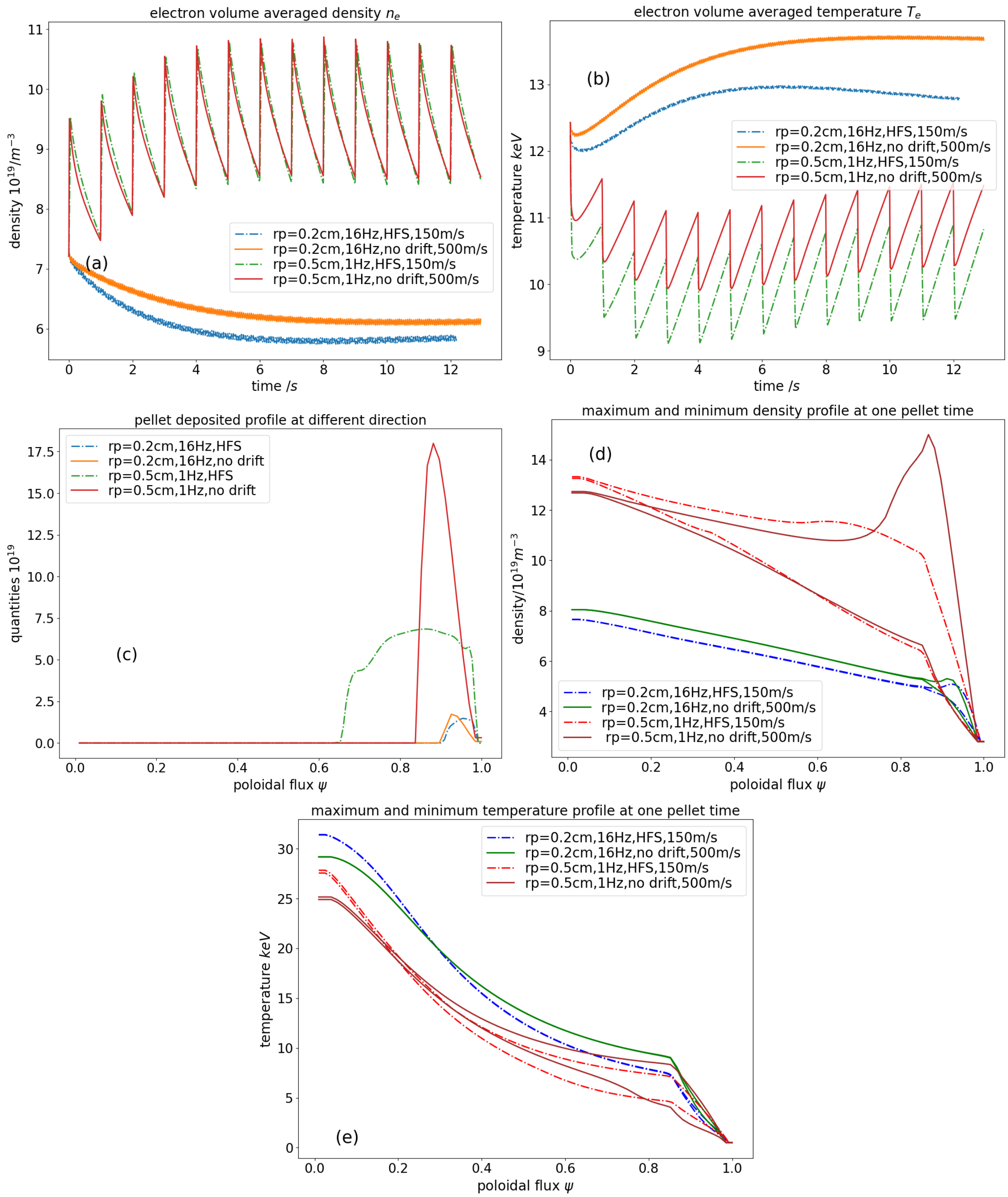

Figure 4: 2mm,16Hz pellet and 5mm,1Hz pellet cases when injected from different direction(a)electron averaged density,(b)electron averaged temperature,(c)pellet deposited profile, (d)maximum and minimum density profile at one pellet time when reach steady state and (e)maximum and minimum temperature profile at one pellet time when reach steady state. The pellet injected velocity is $500m/s$ in no drift case(solid line) and $150m/s$ in HFS(dash dot line).

of $r_p = 2mm$ scenarios is ignorable for tokamak operation. Although the HFS inject velocity ($v_p = 150m/s$) is lower than the no dirft cases ($v_p = 500m/s$), the density at steady state in these two cases are simliar. Relatively, the $r_p = 5mm$ scenarios have lower steady state temperature than $r_p = 2mm$ scenarios. Due to the HFS inward drift, which makes the fuel directly lower the temperature at the center as shown in Fig. 4(c) shown, the temperature of HFS injected cases is much lower than that of no drift case. And to the density perturbation, the $r_p = 5mm$ pellet has a the larger temperature perturbation of 1keV than that for $r_p = 2mm$.

To further estimate the influence of PI on profiles, different steady state density and temperature profiles of one pellet with various sizes are plotted on Fig. 4(d) and Fig. 4(e). The maximum and minimum of profiles clearly show the significant variations due to pellet size. In general, the variations on density and temperature caused by the 5mm pellet are larger than that by the 2mm pellet. The drift effect on the HFS PI deeper the fueling position to make the HFS PI deposited profile more flattened and with much less variations. Another interesting point is that although the no drift 5mm case only fuels at $\psi > 0.8$, it can still efficiently affect the central density as the HFS PI do, due to the large local density gradient caused by the bigger size (5mm) of the pellet. We have found that, in the 5mm no drift case, the lowest temperature profile almost has no pedestal. Therefore, the further consideration is necessary for the 5mm size PI to clarify the influence of pedestal and related MHD instabilities.

4.2.2. The pellet injection depth under the different fueling scenarios As mentioned above, the fueling depth is a key parameter to affect the steady state density and temperature profile. The investigation of the pellet reached fuel depth is shown on Fig. 4(a) (HFS) and Fig. 4(b) (no drift) under different fueling scenario. It can be seen in both Fig. 4(a) and Fig. 4(b) that the fuel depth has almost no dependence on frequency when the pellet size and velocity are fixed in those cases. As be expected, the depth varies approximately linearly with the injection velocity. To the no drift case,the fuel depth is only $rho \sim 0.2$, even at $v_p = 2000m/s$ and $r_p = 5mm$, due to high density and temperature pedestals of CFETR. Although the HFS pellet injection velocity is much lower than that in the no drift case, the HFS fueling deposition depth is much larger than that in the no drift case. The key problem is the pellet size here. In this MHD theory, the drift displacement is proportional to particles quantities. Thus, the HFS drift features give rise to the possibility for deeper fueling into the centeral plasma region in the future reactor.

4.2.3. CFETR performance and burning fraction in different fueling scenarios According to the previous PI fueling experiments, the density was able to achieve 0.8-2.0 n_{GW}[31] without disruption. For robust consideration, we chose the operation region of $0.8 - 1.2n_{GW}$ in this paper. The Fig. 6(a) shows the volume-averaged electron density and volume-averaged ion temperature, and the green area is the safe operation region of $0.8 < n_{GW} < 1.2$ and $T > 10keV$. Almost all the $r_p = 2mm$ cases are located at low density but high temperature region. On the other hand, the bigger size cases

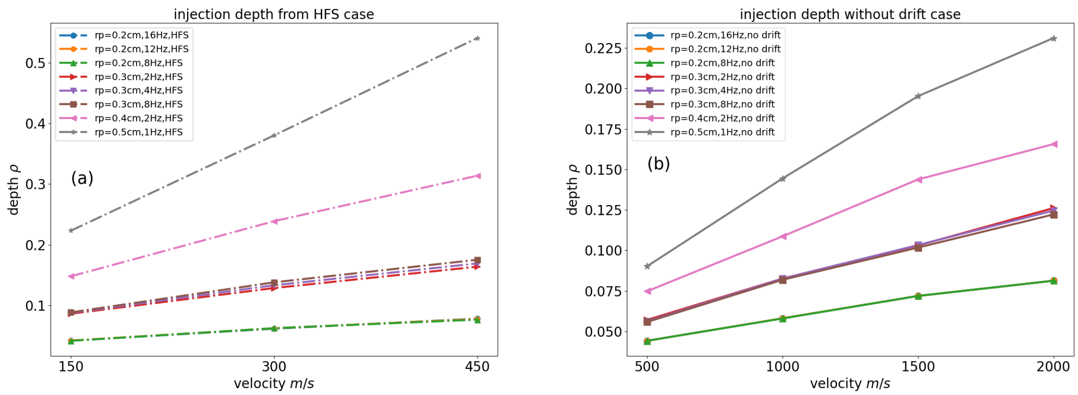

Figure 5: Injection maximum depth under the different scenario:(a)injection depth of HFS(dash dot line) and no drift case(solid line),(b)injection depth of LFS(dash line) and no drift case

of $r_p = 4mm$ and $r_p = 5mm$ with the high velocity or HFS injection may lower the temperature level to as low as 10keV.It however has to be pointed out that, though the low temperature may be a factor to decrease the burning fraction, Fig. 6(b) shows the burning fraction continuing increase with the pellet size and velocity. To understanding this trend, we revisit Eq. (9) where the burning fraction is shown to relate to T_i, γ, and the factor of $10Q/(5+Q)$. Clearly, the effect of fusion power increase is insignificant. For a fusion power increase from 1GW to 1.8GW, i.e. $Q = 12.5$ to 22.5, the contribution of the factor $10Q/(5+Q)$ to the burning fraction only raise from 7.14 to 8.18. Thus, as T_i gets lower, $\tau_p/\tau_E = \frac{1}{\gamma}$ is the only possible cause for the burning fraction increase. The Fig. 6(d) clearly shows it. As the pellet size and velocity increase, the $\frac{1}{\gamma}$ raises from 0.3 to 0.6, a remarkable improvement of particle confinement.

To find the practical fueling regime for CFETR, we further analyse the fueling scenarios by the 1-D model. The region with the >3% burning fraction and the >1GW fusion power is colored yellow in Fig. 6(b), the suitable fueling scenarios for CFETR in these simulations are $r_p = 3mm$, $4Hz$, $1000-2000m/s$, no-drift; $r_p = 5mm$, $1Hz$, $500m/s$, no-drift; $r_p = 3mm$, $4Hz$, $450m/s$, HFS. However, as shown in Fig. 4(c), the large pellet perturbation on profiles is unfavored for operation. Fig. 6(c) shows the positive difference between the maximum and mean densities locally and the corresponding negative temperature difference. The $r_p = 5mm$ PI causes a density perturbation $>4\times10^{19}m^3$, making these fueling scenarios unacceptable. Thus, it seems that one may get only a very narrow parameter regime for CFETR fueling design. However, if we lower the fusion energy gain Q, i.e., either increasing the al heating power or reducing the fusion power expectation, the burning fraction criterion can then be much easily achieved.

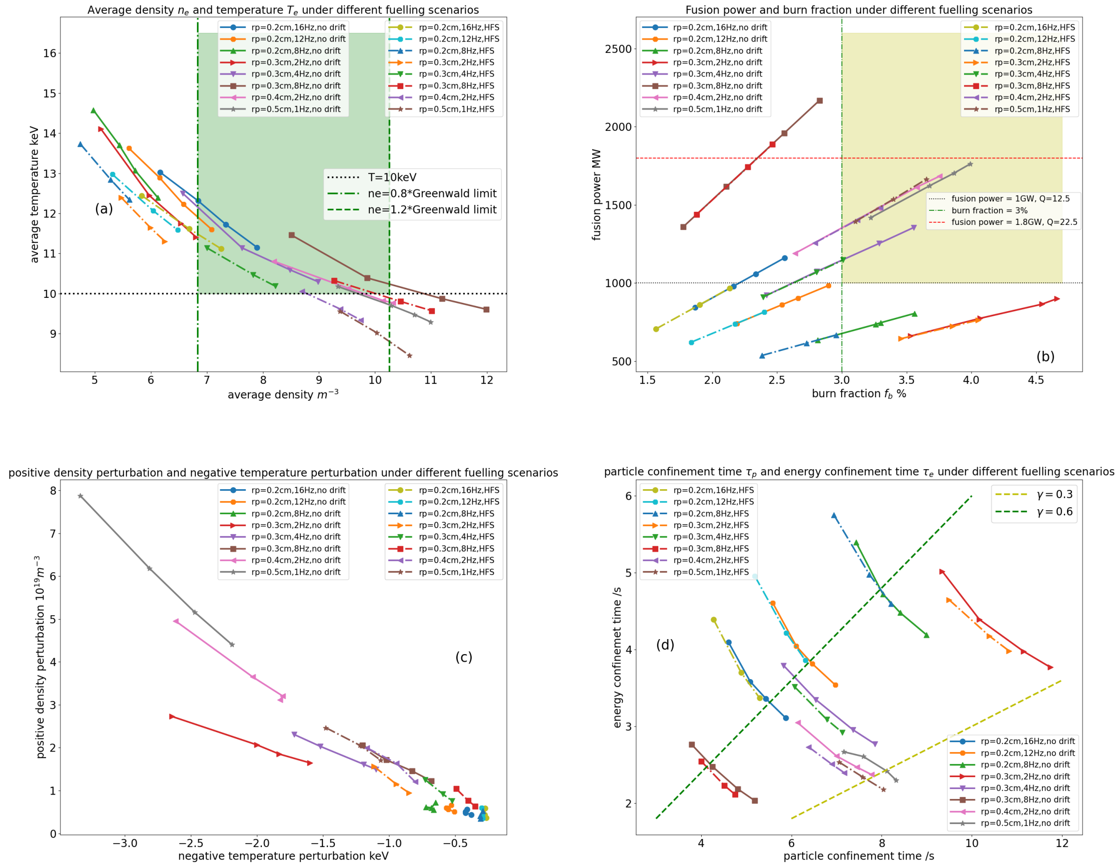

Figure 6: The HFS(dash dot line), LFS(dash line), no drift(solid line) pellet scenario influence on CFETR:(a)Average density and temperature at steady state,(b)Fusion power and burn fraction at steady state, and (c) the fluctuation at positive density and negative temperature after pellet injected. The point from left to right are the result of 500m/s,1000m/s,1500m/s,2000m/s at no drift cases and 150m/s,300m/s,450m/s at HFS cases.

5. Conclusion and Discussion

In summary, this paper offers a 0-D analysis for the burning fraction criterion and a 1-D simulation for favorable fueling scenarios of CFTER, which can also be applied to future DEMOs and fusion power stations.

We start from the zero-dimension burning fraction requirement to make a magnitude estimation for reactor design. Then, a one-dimensional transport model evolving both density and temperature profiles at the same time is developed, with NGS and MHD drift models for PI fueling, based on the framework of BOUT++. Several fueling scenarios are analysed to test designed CFETR burning fraction and performance for 1GW cases. For PI fueling, under a rate of $\sim 1.8\times10^{22}/s$, the cases for the pellet size from 2mm to 5mm with the injection velocity from 500m/s to 2000m/s of no drift and 150m/s to 450m/s of HFS injection, are simulated.

The main conclusion in numerical simulation under designed CFETR parameters are as below:

(a) In the 0-D analysis, the unfavored fueling efficiency or unfavored particle confinement makes the burning fraction requirement as high as the Lawson criterion, hardly being achieved.

(b) In the 1-D transport simulation, the fueling depth almost has no dependence on the PI frequency, when the fueling rate in a certain range. And the fueling depth is approximately linearly varied with the injection velocity, even with the drift being taken into account. In comparison with the no drift case, the HFS drift makes the pellet penetrate deeper even with a slower velocity.

(c) For the 1-D transport, the bigger pellet size and higher velocity can certainly increase the density but reduce the temperature. And the contribution to the burning fraction improvement by increasing pellet size and velocity mainly comes from the improvement of particle confinement.

(d) In 1-D transport simulation, the practical fueling scenario that considers the reasonable burning fraction, high density, high fusion power, and small density perturbation are $r_p = 3mm, 4Hz, nodrift, 1000m/s - 2000m/s; orHFS450m/s$.

Although certain optimistic assumptions such as the 100% fueling efficiency have been made, the 1-D model used in this paper is still applicable for the first-step analysis for CFETR fueling scenarios. Nevertheless, according to the simulation result, only has a narrow region been found in the parameter space for CFETR pellet fueling scenarios. It thus asks for further efforts on improve the model with better approximations and detailed physics, as well as interaction with the background plasma, such as pellet triggered ELM.

6. Acknowledgments

This work is supported by NSFC Grant Nos.11975087, 41674165, National Key Research and Development Program of China Nos.2017YFE0300501 and 2018YFE030310 and by the U.S. DOE by LLNL under Contract No. DE-AC52-07NA27344. LLNL-JRNL-xxxxxx.

References

[1] Abdou M A, Vold E L, Gung C Y, Youssef M Z and Shin K 1986 *Fusion Technology* **9** 250–285 (*Preprint* https://doi.org/10.13182/FST86-A24715) URL https://doi.org/10.13182/FST86-A24715

[2] Abdou M, Riva M, Ying A, Day C, Loarte A, Baylor L, Humrickhouse P, Fuerst T F and Cho S 2020 *Nuclear Fusion* **61** 013001 URL https://doi.org/10.1088/1741-4326/abbf35

[3] Wan Y, Li J, Liu Y, Wang X, Chan V, Chen C, Duan X, Fu P, Gao X, Feng K, Liu S, Song Y, Weng P, Wan B, Wan F, Wang H, Wu S, Ye M, Yang Q, Zheng G, Zhuang G and and Q L 2017 *Nuclear Fusion* **57** 102009 URL https://doi.org/10.1088%2F1741-4326%2Faa686a

[4] Miyazawa J, Masuzaki S, Yamada H, Suzuki H, Goto M, Morita S, Murakami S, Narihara K, Osakabe M, Peterson B, Sakakibara S, Tanaka K, Kaneko O, Komori A, Matsuoka K and

Motojima O 2003 *Journal of Nuclear Materials* **313-316** 534 – 538 ISSN 0022-3115 plasma-Surface Interactions in Controlled Fusion Devices 15 URL http://www.sciencedirect.com/science/article/pii/S0022311502014575

[5] Yuan X, Li J, Wu J, Li J, Chen Y, Zhuang H, Zhou Y, Zheng X W and Hu J 2018 *Fusion Engineering and Design* **134** 62 – 67 ISSN 0920-3796 URL http://www.sciencedirect.com/science/article/pii/S0920379618305441

[6] Pégourié B 2007 *Plasma Physics and Controlled Fusion* **49** R87–R160 URL https://doi.org/10.1088%2F0741-3335%2F49%2F8%2Fr01

[7] Raman R, Martin F, Quirion B, St-Onge M, Lachambre J L, Michaud D, Sawatzky B, Thomas J, Hirose A, Hwang D, Richard N, Côté C, Abel G, Pinsonneault D, Gauvreau J L, Stansfield B, Décoste R, Côté A, Zuzak W and Boucher C 1994 *Phys. Rev. Lett.* **73**(23) 3101–3104 URL https://link.aps.org/doi/10.1103/PhysRevLett.73.3101

[8] Wang S and Wang S 2016 *Plasma Science and Technology* **18** 1155–1161 URL https://doi.org/10.1088%2F1009-0630%2F18%2F12%2F03

[9] Takenaga H, Asakura N, Shimizu K, Nagashima K, Kubo H and Sakasai A 1997 *Journal of Nuclear Materials* **241-243** 569 – 573 ISSN 0022-3115 URL http://www.sciencedirect.com/science/article/pii/S0022311597801018

[10] Boyer M D and Schuster E 2014 *Plasma Physics and Controlled Fusion* **56** 104004 URL https://doi.org/10.1088%2F0741-3335%2F56%2F10%2F104004

[11] on Confin Transport I P E G, on Confin Database I P E G and Editors I P B 1999 *Nuclear Fusion* **39** 2175–2249 URL https://doi.org/10.1088%2F0029-5515%2F39%2F12%2F302

[12] Lin W, Wang X, Xiao C, Wang Z, Kong D and Lang Y 2020 *Nuclear Fusion* **60** 076007 URL https://doi.org/10.1088%2F1741-4326%2Fab8c64

[13] Mantica P, Angioni C, Bonanomi N, Citrin J, Grierson B A, Koechl F, Mariani A, Staebler G M, , and and 2019 *Plasma Physics and Controlled Fusion* **62** 014021 URL https://doi.org/10.1088%2F1361-6587%2Fab5ae1

[14] Braginskii S I 1965 *Reviews of Plasma Physics* **1** 205

[15] 2012 *Fusion Physics* Non-serial Publications (Vienna: INTERNATIONAL ATOMIC ENERGY AGENCY) ISBN 978-92-0-130410-0 URL https://www.iaea.org/publications/8879/fusion-physics

[16] (prepared by PR Thomas) J T 1999 *Nuclear Fusion* **39** 1619–1625 URL https://doi.org/10.1088%2F0029-5515%2F39%2F11y%2F301

[17] Xie H, Chan V S, Ding R, Shi N, Jian X, Zagórski R, Ivanova-Stanik I, Chen J, Chen J and and J L 2020 *Nuclear Fusion* **60** 046022 URL https://doi.org/10.1088/1741-4326/ab742b

[18] Meneghini O, Smith S, Lao L, Izacard O, Ren Q, Park J, Candy J, Wang Z, Luna C, Izzo V, Grierson B, Snyder P, Holland C, Penna J, Lu G, Raum P, McCubbin A, Orlov D, Belli E, Ferraro N, Prater R, Osborne T, Turnbull A and Staebler G 2015 *Nuclear Fusion* **55** 083008 URL https://doi.org/10.1088%2F0029-5515%2F55%2F8%2F083008

[19] Candy J, Holland C, Waltz R E, Fahey M R and Belli E 2009 *Physics of Plasmas* **16** 060704 (*Preprint* https://doi.org/10.1063/1.3167820) URL https://doi.org/10.1063/1.3167820

[20] Staebler G M, Kinsey J E and Waltz R E 2007 *Physics of Plasmas* **14** 055909 (*Preprint* https://doi.org/10.1063/1.2436852) URL https://doi.org/10.1063/1.2436852

[21] Angioni C and Peeters A G 2008 *Physics of Plasmas* **15** 052307 (*Preprint* https://doi.org/10.1063/1.2913610) URL https://doi.org/10.1063/1.2913610

[22] Chen J, Jian X, Chan V S, Li Z, Deng Z, Li G, Guo W, Shi N, Chen X and Team C P 2017 *Plasma Physics and Controlled Fusion* **59** 075005 URL https://doi.org/10.1088%2F1361-6587%2Faa6d20

[23] Dudson B, Umansky M, Xu X, Snyder P and Wilson H 2009 *Computer Physics Communications* **180** 1467 – 1480 ISSN 0010-4655 URL http://www.sciencedirect.com/science/article/pii/S0010465509001040

[24] Lang P, Gafert J, Gruber O, Kaufmann M, Lorenz A, Maraschek M, Mertens V, Neuhauser J, Salzmann H and Team A U 2000 *Nuclear Fusion* **40** 245–260 URL https://doi.org/10.1088/0029-5515/40/2/308
[25] Baylor L, Geraud A, Houlberg W, Frigione D, Gadeberg M, Jernigan T, Kloe J D, Kupschus P, Kuteev B, Lang P, Oomens A, Qualls A, Sato K and Schmidt G 1997 *Nuclear Fusion* **37** 445–450 URL https://doi.org/10.1088%2F0029-5515%2F37%2F4%2Fi02
[26] Parks P B and Turnbull R J 1978 *The Physics of Fluids* **21** 1735–1741 (*Preprint* https://aip.scitation.org/doi/pdf/10.1063/1.862088) URL https://aip.scitation.org/doi/abs/10.1063/1.862088
[27] Lang P T, Büchl K, Kaufmann M, Lang R S, Mertens V, Müller H W and Neuhauser J 1997 *Physical Review Letters* **79** 1487–1490 URL https://doi.org/10.1103%2Fphysrevlett.79.1487
[28] Polevoi A R and Shimada M 2001 *Plasma Physics and Controlled Fusion* **43** 1525–1533 URL https://doi.org/10.1088%2F0741-3335%2F43%2F11%2F307
[29] Matsuyama A, Koechl F, Pégourié B, Sakamoto R, Motojima G and Yamada H 2012 *Nuclear Fusion* **52** 123017 URL https://doi.org/10.1088/0029-5515/52/12/123017
[30] Parks P B and Baylor L R 2005 *Phys. Rev. Lett.* **94**(12) 125002 URL https://link.aps.org/doi/10.1103/PhysRevLett.94.125002
[31] Baylor L, Parks P, Jernigan T, Caughman J, Combs S, Foust C, Houlberg W, Maruyama S and Rasmussen D 2007 *Nuclear Fusion* **47** 443–448 URL https://doi.org/10.1088%2F0029-5515%2F47%2F5%2F008

Appendix

Appendix A.

According to classical slowing down theory[15], slowing down time can be estimated:

$$\tau_s = \frac{\tau_{se}}{3} \ln \frac{W_{b0}^{1.5} + W_c^{1.5}}{W_{th,i}^{1.5} + W_c^{1.5}} \tag{A.1}$$

$$\tau_{se} = \frac{0.2 A_b T_e^{1.5}[keV]}{Z_b n_e [10^{20} m^{-3}] \ln \Lambda} \tag{A.2}$$

$$W_c = 14.8 \overline{Z}^{2/3} \overline{A}_b^{1/3} T_e \tag{A.3}$$

$$f_\alpha(W_\alpha) = \frac{\tau_{se} \left\langle \sigma_{DT} v \right\rangle n_D n_T}{2W_\alpha (1 + (\frac{W_c}{W_{\alpha 0}})^{\frac{3}{2}})} \tag{A.4}$$

where the $f_\alpha(W_\alpha)$ is the energy distribution of alpha. And classical heat transport time:

$$Q_s = \frac{3}{2} n_s \sum_\beta \nu_{s\beta}(T_\beta - T_s) \tag{A.5}$$

$$\nu_{s\beta} = 1.8 \times 10^{-19} \frac{(m_s m_\beta)^{1/2} Z_s^2 Z_\beta^2 n_\beta \lambda_{s\beta}}{({}_s T_\beta + m_\beta T_s)^{3/2}} \; sec^{-1} \tag{A.6}$$

The alpha heating power on electron and background ion(take D as an example) are as follows:

$$P_e = n_D n_T \left\langle \sigma \nu \right\rangle (E_{\alpha 0} - kT_{He}) \frac{F_i}{F_i + F_e} \tag{A.7}$$

$$P_{\alpha D} = \nu_{\alpha D} * P_i/(\nu_{\alpha D} + \nu_{\alpha T} + \nu_{\alpha He}) \tag{A.8}$$

$$F_i = \int_0^{3.5MeV} W_\alpha f(W_\alpha) dW_\alpha \tag{A.9}$$

$$F_e = \int_0^{3.5MeV} W_c^{3/2} f(W_\alpha)/W_\alpha^{1/2} dW_\alpha \tag{A.10}$$

where $W_{\alpha 0} = 3.5MeV$ is alpha born energy.